A Dedicated ARAIM Ground Monitor to Validate the Integrity Support Message

Yawei Zhai, Shahriar Kiarash, Michael Jamoom, *Illinois Institute of Technology*
Mathieu Joerger, *The University of Arizona*
Boris Pervan, *Illinois Institute of Technology*

BIOGRAPHY

Yawei Zhai obtained a Bachelor's degree in Mechanical Engineering from Qingdao University of Science and Technology, China, in 2013. He is currently a Ph.D. candidate and Research Assistant in Mechanical and Aerospace Engineering at the Illinois Institute of Technology (IIT). His research focuses on advanced receiver autonomous integrity monitoring (ARAIM) fault detection and exclusion (FDE) using multi-constellation global navigation satellite systems (GNSS).

Shahriar Kiarash is senior undergraduate student in Aerospace Engineering with a minor in Computer Science at IIT. He is expected to receive his B.S in May 2018. He was also dean's student list nominee in 2015. He joined the Navigation Lab in 2017 and is passionate about GNSS and navigation field. He is currently completing an internship at Continental AG.

Dr. Michael Jamoom received his B.S. in Astronautical Engineering from the US Air Force Academy, in 1997, M.S. in Aeronautics and Astronautics from the Massachusetts Institute of Technology, in 1999, and Ph.D. in Mechanical and Aerospace Engineering from the Illinois Institute of Technology, in 2016. From 1997 to 2008, he served active duty in the Air Force, primarily as a KC-135 Instructor Pilot. From 2006-2008, he was the AFOTEC KC-X Test Director, where he developed the operational test plan for the Air Force's air refueling tanker replacement. From 2008-2010, he was a Military Operations Analyst for Systems, Planning, and Analysis Inc., where he performed operations research analysis for the Joint Staff in the Pentagon. From 2010 to the present, he serves in the Air Force Reserves as a KC-135 Instructor Pilot with over 3900 hours of flying experience. He is also currently a Senior Research Associate in Mechanical and Aerospace Engineering at the Illinois Institute of Technology (IIT) Navigation Lab, focused on Unmanned Aircraft System Detect and Avoid research. Dr. Jamoom is a member of AIAA and of the Institute of Navigation (ION).

Dr. Mathieu Joerger obtained a Diplôme d'Ingénieur in Mechatronics from the Ecole Nationale Supérieure des Arts et Industries de Strasbourg, France, in 2002, and a M.S. and a Ph.D. in Mechanical and Aerospace Engineering from the Illinois Institute of Technology (IIT), in 2002 and 2009 respectively. He is the 2009 recipient of the Institute of Navigation (ION) Parkinson award, and the 2014 recipient of the ION's Early Achievement Award. He is currently an assistant professor at The University of Arizona, working on multi-sensor integration, sequential fault-detection for multi-constellation navigation systems, and relative and differential receiver autonomous integrity monitoring (RAIM).

Dr. Boris Pervan is a Professor of Mechanical and Aerospace Engineering at IIT, where he conducts research on advanced navigation systems. Prior to joining the faculty at IIT, he was a spacecraft mission analyst at Hughes Aircraft Company (now Boeing) and a postdoctoral research associate at Stanford University. Prof. Pervan received his B.S. from the University of Notre Dame, M.S. from the California Institute of Technology, and Ph.D. from Stanford University. He is an Associate Fellow of the AIAA, a Fellow of the Institute of Navigation (ION), and Editor-in-Chief of the ION journal NAVIGATION. He was the recipient of the IIT Sigma Xi Excellence in University Research Award (2011, 2002), Ralph Barnett Mechanical and Aerospace Dept. Outstanding Teaching Award (2009, 2002), Mechanical and Aerospace Dept. Excellence in Research Award (2007), University Excellence in Teaching Award (2005), IEEE Aerospace and Electronic Systems Society M. Barry Carlton Award (1999), RTCA William E. Jackson Award (1996), Guggenheim Fellowship (Caltech 1987), and Albert J. Zahm Prize in Aeronautics (Notre Dame 1986).

ABSTRACT

Future dual-frequency, multi-constellation advanced receiver autonomous integrity monitoring (ARAIM) is expected to bring significant navigation performance improvement to civil aviation. The ARAIM user algorithm, which includes fault detection and exclusion (FDE) functions, is autonomously executed at the airborne receiver. To achieve specific integrity and continuity requirements, the real-time FDE process requires assertions on the signal-in-space (SIS) performance, and this information is carried in the integrity support message (ISM). This paper describes the design, analysis, and evaluation of the offline ground monitor, which aims at validating the ISM broadcast to users. To achieve this, GNSS satellite orbits and clocks must be estimated. There are many sophisticated orbit determination processes such as the one used by the international GNSS service (IGS), whose performance is specified in terms of accuracy. In contrast, the proposed offline ARAIM architecture is mainly intended for safety-critical aviation applications, in which integrity is of the primary concern. This monitor employs a straightforward approach to estimate satellite orbit/clock, which aims at facilitating ISM generation and validation. It takes advantage of the existing satellite based augmentation system (SBAS) ground infrastructure. In this paper, a worldwide network of sparsely distributed reference stations is considered, and parametric satellite orbital models are employed in the estimators, whose derivation and implementation are described step by step. Two separate analyses, covariance analysis and model fidelity evaluation, are carried out to respectively assess the impact of measurement errors and of residual model errors on the monitor's estimated orbit/clock. We have investigated different orbit models (GPS legacy versus CNAV orbital model) and reference station clock models (quadratic model versus no model). The results indicate the standard deviation of the monitor's orbit/clock estimation error is on the order of 30 cm, which is adequate for SIS performance validation.

INTRODUCTION

The main challenge when using global navigation satellite systems (GNSS) in safety-critical civil aviation applications is to mitigate the integrity threats caused by measurement faults, including satellite and constellation failures [1]. For the single constellation case, using the global positioning system (GPS) only, fault detection (FD) can be implemented using receiver autonomous integrity monitoring (RAIM). RAIM has been implemented since the mid-1990s as a backup navigation tool to support aircraft en-route flight using GPS only [2-4]. The core principle of RAIM is to exploit redundant measurements to achieve self-contained FD at the user receiver [5].

After decades of worldwide development, two key elements have been foreseen in future GNSS. First, nominal measurement errors will be significantly reduced using dual-frequency signals, which will remove the largest source of error—ionospheric delay. Second, four constellations including GPS (U.S.), GLONASS (Russia), Galileo (European Union) and Beidou (China) are expected to finish their modernizations and/or full deployments in the near term [6], which will provide many more satellites in view than we have available today using GPS alone. These revolutionary developments in GNSS, together with important advancements in the RAIM concept, will open the possibility to independently support aircraft navigation using GNSS, from en-route flight towards final approach to landing, with minimal investment in ground infrastructure. Therefore, considerable effort has recently been expended, especially in the European Union and in the United States [7, 8], to develop new dual-frequency, multi-constellation advanced RAIM (ARAIM) fault detection and exclusion (FDE) methods.

The performance of RAIM/ARAIM is measured either in terms of integrity risk or in terms of protection level (PL). It is highly dependent on the assumed GNSS nominal signal-in-space (SIS) error models and on the a-priori fault probabilities. In current conventional RAIM implementations, this information is defined by the GPS constellation service provider (CSP) commitments, and is hardcoded in the receiver. As an evolution of RAIM, ARAIM will (a) additionally use constellations that are not as mature as GPS, and (b) seek to provide assured navigation for vertical guidance. To provide flexibility in the evolution of RAIM to multi-constellation ARAIM, and to minimize invasiveness into the avionics, ARAIM will include an integrity support message (ISM). The ISM will carry information defining SIS error and fault statistics, including nominal measurement biases, standard deviations of the ephemeris and clock errors, prior probabilities of satellite faults, and prior probabilities of constellation-wide faults [7]. The ISM parameters will be generated and validated at the ground, and updated to users as needed. Various methods of ISM dissemination are presently being considered, including on-aircraft databases and data broadcast through geosynchronous satellites or one or more of the GNSS core constellations. The methods and result described are applicable regardless of method of dissemination.

To validate the ISM, 'online' and 'offline' ARAIM architectures have been under investigated [9, 10]. Offline architectures have generally been perceived as preferable because they do not require a real-time communication link between users and ground segment, and therefore eliminates the connectivity risk [9]. An offline ARAIM monitor would rely on post-processed GNSS measurements to bound errors in CSP broadcast navigation message on a long-term basis [9]. To do this, prior research has taken truth satellite positions and clock biases from the international GNSS service (IGS) network [11-13]. However, given that ARAIM is intended to operate over several decades, monitor dependence on external systems or organizations with little or no stake in civil aviation must be carefully considered, and ideally, avoided. Most importantly, ARAIM will serve safety critical applications, any potential safety risks must be properly accounted for and quantified. The IGS, the national geospatial intelligence agency (NGA), and others currently provide high-accuracy satellite orbit/clock products. But none of these agencies make specific commitments on the reliability of their products, or on the processes used to obtain those products. Further, data gaps exist in those products, especially during satellite fault events, which are crucial to ARAIM. In response, this paper develops a new approach to define and validate ISM parameters by designing a dedicated ARAIM offline ground monitor architecture.

This new monitor employs a simple and transparent orbit determination process to estimate satellite orbits/clocks. Measurements are collected from a worldwide network of sparsely distributed reference stations (RS). A parametric orbit model is used to fit data over time. Because most satellite faults are caused by clock anomalies, the standard quadratic clock model is not applied for satellite clocks. In contrast, an RS can be equipped with redundant atomic clocks, so any receiver clock faults can be detected removed in post-processing. Therefore, as an alternative to directly estimating instantaneous RS clocks states at each time-epoch, we also investigate the benefit of using quadratic RS receiver clock models. Two estimators will be considered: a batch least-squares method, and a Kalman Filter (KF). In both cases, satellite orbit, satellite clocks, and RS clocks will be simultaneously estimated over a four-hour fit interval supported by both the GPS legacy and GPS CNAV orbit models.

Satellite orbit and clock errors are determined by differencing the positioning and timing solution derived from the GNSS-broadcast navigation message and the estimates generated by the offline monitor. This data will provide the means to evaluate the ISM parameters. On the one hand, we desire that these parameters include enough margin to bound the actual constellation performance over the specified period of ISM validity (e.g., one month). On the other hand, the ISM parameters should not be set too conservatively or ARAIM availability will degrade. Therefore, it is essential that the ground monitor be capable of producing accurate satellite position and clock estimates. In this work, a two-step evaluation of the monitor's orbit and clock estimate accuracy is carried out: first, the impact of measurement errors at RS receivers is quantified by covariance analysis, and second, the fidelity of the orbit model is validated by computing the residual errors relative to known satellite positions.

Four scenarios are considered in performance evaluations: (a) GPS legacy versus CNAV orbit models, and (b) quadratic model versus no model for RS receiver clocks. In regard to (a), using the more sophisticated CNAV model can reduce residual fitting errors, but it may also increase the standard deviations of the estimated satellite positions (because more parameters need to be estimated) [14]. In regard to (b), direct estimation of instantaneous RS clocks eliminates clock model fidelity errors and provides robustness against RS clock faults, but standard deviations of estimation errors may increase because each clock estimate is instantaneous in time (earlier measurements can't be used). In the analysis, the worst-case SIS ranging error (SISRE) is derived to conservatively quantify the resulting estimate errors in the along-track, cross-track, radial and clock components.

REQUIRED OFFLINE MONITOR PERFORMANCE

Using an offline monitor, the update rate of the ISM may vary from a month to year depending on the need [9]. A large amount of data will be processed at the ground to obtain the ISM, which is expected to bound the SIS performance until the next update. To achieve this, differences between broadcast ephemeris and the monitor's estimated satellite orbit/clock will be first evaluated over time, and then these will be used to validate (or modify, if needed) the ISM parameter values. In this paper, we focus mainly on producing satellite orbit and clock estimates to validate b_{nom} and σ_{URA}, which specify a Gaussian bound on the SIS performance under nominal conditions, (i.e., no faults). Since the monitor's orbit/clock estimation errors will directly contribute to our ability validate ISM, it is necessary to first define the required accuracy of the monitor's orbit/clock estimator.

Equation (1) shows the relationship among the actual standard deviation of broadcast satellite orbit/clock error σ_{ACTUAL} (actual σ_{URA}), the standard deviation of the monitor's estimated orbit/clock error $\sigma_{MONITOR}$, and the validated standard deviation of the satellite orbit/clock error $\sigma_{VALIDATE}$ (validated σ_{URA}).

$$\sigma_{VALIDATE} = \sqrt{\sigma_{ACTUAL}^2 + \sigma_{MONITOR}^2} \quad (1)$$

Figure 1 plots $\sigma_{VALIDATE}$ versus $\sigma_{MONITOR}$ over different σ_{ACTUAL} values. For example, the figure shows that for σ_{URA} = 2.4 m, which is the current minimum value that the GPS CSP is willing to commit to, having $\sigma_{MONITOR}$ is less than 1.73 m is sufficient for validation. According to the most recent study on GPS SIS performance to support ARAIM, the maximum actual σ_{URA} is observed on space vehicle number (SVN) 61, where σ_{ACTUAL} is 1.65 m, and for most satellites it is much smaller [13]. The red curve is of most interest because it is expected future performance of the GPS constellation will provide σ_{ACTUAL} of 1 m, or less. And dual-constellation ARAIM availability simulations have revealed localizer performance with vertical guidance (LPV)-200 approach can only be supported when σ_{ACTUAL} of both constellations are approximately 1 m [9]. The figure shows slow growth of $\sigma_{VALIDATE}$ as $\sigma_{MONITOR}$ increases. Even when $\sigma_{MONITOR}$ reaches half of σ_{ACTUAL} at the end of the curve, the achievable validated σ_{URA} is still around 1.1 m.

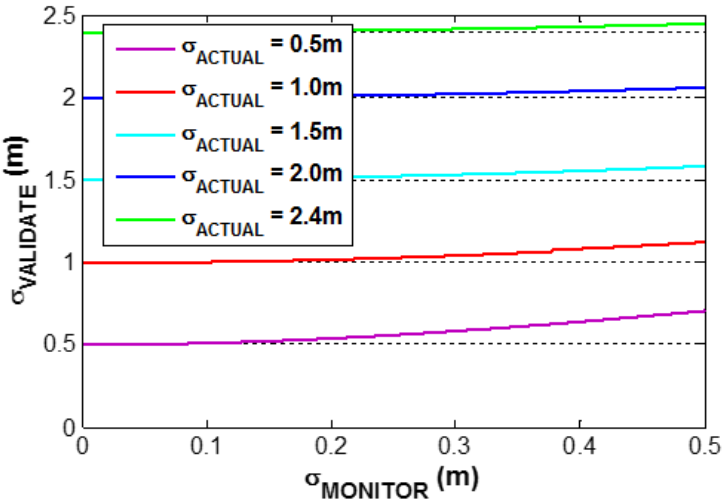

Fig. 1 $\sigma_{VALIDATE}$ vs. $\sigma_{MONITOR}$ over Varying σ_{ACTUAL} Values

In addition to $\sigma_{MONITOR}$, the estimated satellite orbit/clock error may have a non-zero mean, denoted by $b_{MONITOR}$. This term is accounted as one component of the validated ISM parameter, b_{nom}. However, using baseline solution separation ARAIM user algorithm [7], the absolute value of b_{nom} is additive for each measurement. This causes the integrity risk bound to become loose as the number of measurements increases, thereby degrading availability performance [7]. Therefore, it is desirable to mitigate any contributions of $b_{MONITOR}$ to the validated b_{nom}.

From the analysis and discussion above, it can be seen that the required accuracy of the offline monitor is significantly lower than the precise satellite orbit/clock products by IGS or NGA. Instead, it is the reliability of the monitor's estimator output that is key. In other words, even though the monitor's satellite orbit/clock estimates may have larger errors, their stable performance and consistent availability enables validate ISMs without missing data gaps. Therefore, in the estimator design it is not necessary to pursue a complicated orbit determination process. We can instead the simple, transparent approach described in the next section.

OFFLINE MONITOR ARCHITECTURE

This section describes the offline monitor architecture step-by-step. A network of worldwide sparsely distributed RS is employed to collect code and carrier measurements over time. In the selection of sites for the RS, we take advantage of the satellite based augmentation system (SBAS) ground infrastructures since they are already existing and are designed to support civil aviation applications. Figure 2 (left) shows all of the existing SBAS RS from different countries or regions, and Figure 2 (right) shows the network of 20 RS used in this work. To obtain a roughly uniform global distribution, five non-SBAS RS sites are added. This network ensures that each satellite can continuously be tracked by at least two reference stations, but does not allow reverse

positioning (four RS simultaneously observing a space vehicle (SV) are required to directly estimate the satellite position). Instead, the offline monitor uses parametric orbit models to determine SV trajectories.

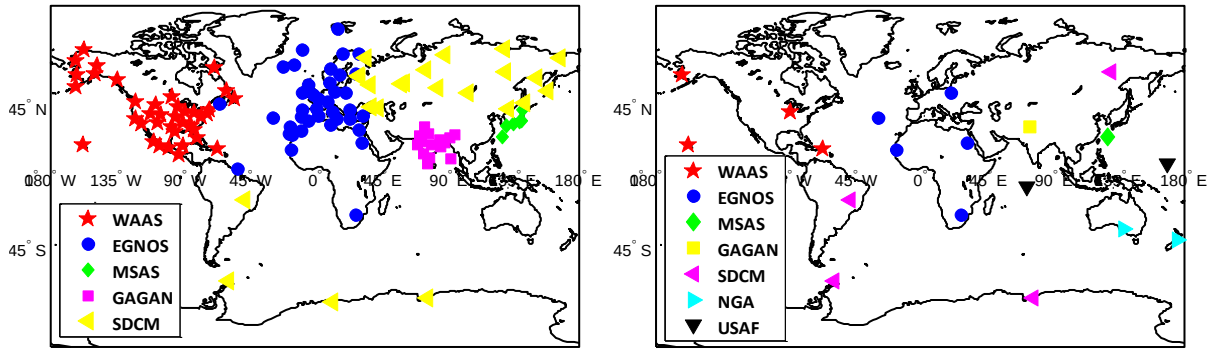

Fig. 2 All Existing SBAS Stations (Left) and Example Network of 20 RS Used in This Work (Right)

Two candidate GPS orbit models, legacy and CNAV, are investigated. Both models are valid for medium earth orbit (MEO) SVs, with 15 orbit parameters being used for legacy model and 17 parameters for CNAV model [15]. Throughout this paper, we assume no satellite maneuvers occur, because the orbit models will not be valid while the spacecraft is thrusting. Maneuvers occur rarely, and they can be handled by simply initiating a new estimator after the maneuver. However, these details of practical implementation are beyond the scope of this work and will not be considered further.

Let $\mathbf{p}_i^{orb}$ be the 15×1 (or 17×1, depending on which orbit model is used) vector of orbit model parameters for SV *i*, and let $\mathbf{g}_{orb,k}$ be the non-linear function that determines SV orbit. The true SV position $\mathbf{x}_{i,k}$ of SV *i* at time epoch *k* can be expressed as:

$$\mathbf{x}_{i,k} = \mathbf{g}_{orb,k}(\mathbf{p}_i^{orb}) + \mathbf{v}_{i,k}^{orb} \tag{2}$$

where $\mathbf{v}_{i,k}^{orb}$ is the deviation of the model output from the true position $\mathbf{x}_{i,k}$. $\mathbf{v}_{i,k}^{orb}$ represents the model's inability to perfectly capture the true orbit, and this it will be further analyzed in later sections. The GPS orbit model is valid over a four-to-six-hour time interval noted T_{FIT} [15]. Sensitivity to T_{FIT} has been evaluated in our prior work in [14]. We use a four-hour fitting interval, which is the most common value for GPS ephemeris.

Both RS and SV are equipped with atomic clocks, and a quadratic polynomial is usually employed to model their nominal errors. However, most SV faults are caused by their clocks, and for the monitor to clearly observe them, no assumption can be made on the SV clock dynamics. As for the RS, whose clock faults can be detected at the ground, it is feasible to apply quadratic clock model. To assess the potential benefit of using such a model for the RS clocks, we analyze two cases: (a) applying a quadratic polynomial to model RS clock errors, and (b) making no assumption on RS clocks, (i.e., punctually estimate RS clock states). Under the scenario of (a), let $b_{j,k}$ to be the clock bias of RS *j* at time *k*; it can be modeled as:

$$b_{j,k} = g_{clk,k}(\mathbf{p}_j^{clk}) + v_{j,k}^{clk} \tag{3}$$

Similar to equation (2), $\mathbf{p}_j^{clk}$ in equation (3) is the 3×1 vector of clock parameters including a_{f0}^j, a_{f1}^j, a_{f2}^j [15], and $v_{j,k}^{clk}$ is the clock model error. $g_{clk,k}(\mathbf{p}_j^{clk})$ is a linear function (in the clock parameters) that can be expressed as:

$$g_{clk,k}(\mathbf{p}_j^{clk}) = a_{f0}^j + a_{f1}^j(t_k - t_{ref}) + a_{f2}^j(t_k - t_{ref})^2 \tag{4}$$

where t_k and t_{ref} are respectively the true time and reference time.

Dual-frequency, ionosphere-free code and carrier measurements for SV *i*, from RS *j*, at time epoch *k*, are expressed by the following two equations:

$$ {}^{i,j}\rho_k = \left\| \mathbf{x}_j - \mathbf{x}_{i,k} \right\| - \tau_{i,k} + b_{j,k} + {}^{i,j}\varepsilon_{tropo,k} + {}^{i,j}\varepsilon_{RNM,\rho,k} \tag{5} $$

$$ {}^{i,j}\varphi_k = \left\| \mathbf{x}_j - \mathbf{x}_{i,k} \right\| - \tau_{i,k} + b_{j,k} + {}^{i,j}\eta + {}^{i,j}\varepsilon_{tropo,k} + {}^{i,j}\varepsilon_{RNM,\varphi,k} \tag{6} $$

where

$\mathbf{x}_j$: known location of RS *j*, for example, in an Earth-Centered Earth-Fixed (ECEF) reference frame

$\mathbf{x}_{i,k}$: unknown location of SV *i* at time *k*

$\tau_{i,k}$: unknown clock offset of SV *i* at time *k*

$b_{i,k}$: unknown clock offset of RS *j* at time *k*

${}^{i,j}\eta$: unknown, constant carrier phase cycle ambiguity for SV *i* at RS *j*

$\| \ \|$: Euclidean norm operator, in this case providing the distance between RS *j* and SV *i*.

The error terms in equations (5) and (6) account for residual tropospheric delay noted ${}^{i,j}\varepsilon_{tropo,k}$, and receiver noise and multipath (RNM) errors denoted by ${}^{i,j}\varepsilon_{RNM,\rho,k}$ for code and ${}^{i,j}\varepsilon_{RNM,\varphi,k}$ for carrier. We assume raw code and carrier measurement RNM error standard deviations of 0.5 m and 0.01 m, respectively. These standard deviations are multiplied by 2.588 to account for the ionosphere-free combination at L1 and L5 frequencies. To account for the temporal and spatial correlation of zenith tropospheric deal (ZTD), a first order Gauss-Markov process with a two-hour correlation time is applied. Assuming the RS have access to data from weather stations, we use the value of 0.05 m as the standard deviation of residual ZTD. This value is scaled for lower elevation satellites using the tropospheric mapping function given in [7, 9].

To estimate the SV orbit parameters and clocks, the measurement equations (5) &. (6) and the orbit/clock model equations (3) & (4) need to be linearized and incorporated into one filter. For illustrative purposes, we will only show code measurement in the following derivations. The code measurement equation (5) is first linearized at $\mathbf{x}^*_{i,k}$:

$$ {}^{i,j}\delta\rho_k = {}^{i,j}\mathbf{e}_k^T \, \boldsymbol{\delta}\mathbf{x}_{i,k} - \tau_{i,k} + b_{j,k} + {}^{i,j}\varepsilon_{\rho,k} \tag{7} $$

where

δ : deviation from nominal values, e.g., $\delta\mathbf{x}_{i,k} = \mathbf{x}_{i,k} - \mathbf{x}^*_{i,k}$

${}^{i,j}\mathbf{e}_k$: 3×1 line of sight (LOS) vector between SV *i* and RS *j* at time *k* in ECEF

${}^{i,j}\varepsilon_{\rho,k}$: code measurement error, including ${}^{i,j}\varepsilon_{tropo,k}$ and ${}^{i,j}\varepsilon_{RNM,\rho,k}$.

In the next step, the orbit model is linearized at ${}^*\mathbf{p}_i^{orb}$ where $\mathbf{x}^*_{i,k} = \mathbf{g}_{orb,k}({}^*\mathbf{p}_i^{orb})$. Substituting the linearized orbit model equation and the clock error model equation (4) into the code measurement, equation (7) becomes:

$$ {}^{i,j}\delta\rho_k = {}^{i,j}\mathbf{e}_k^T \, \mathbf{A}_{i,k}^{orb} \, \boldsymbol{\delta}\mathbf{p}_i^{orb} - \tau_{i,k} + \mathbf{A}_{j,k}^{clk} \, \mathbf{p}_j^{clk} + {}^{i,j}\varepsilon_{\rho,k} \tag{8} $$

where

$\mathbf{A}_{i,k}^{orb}$: Jacobian matrix for the SV orbit model in equation (2), which is 3×15 for the GPS legacy orbit model and 3×17 for the CNAV model. It is composed of numerically-derived partial derivatives of the position coordinates of SV *i* at time *k* $\mathbf{x}_{i,k} = [x_{i,k} \quad y_{i,k} \quad z_{i,k}]^T$ with respect to the orbit parameters $\mathbf{p}_i^{orb} = [p_1 \quad \cdots \quad p_{15}]^T$:

$$\mathbf{A}_{i,k}^{orb} = \begin{bmatrix} \partial x_{i,k}/\partial p_1 & \partial y_{i,k}/\partial p_1 & \partial z_{i,k}/\partial p_1 \\ \vdots & \vdots & \vdots \\ \partial x_{i,k}/\partial p_{15} & \partial y_{i,k}/\partial p_{15} & \partial z_{i,k}/\partial p_{15} \end{bmatrix}^T$$

$\mathbf{A}_{j,k}^{clk}$: 1×3 vector that express equation (4) in a more compact form: $\mathbf{A}_{j,k}^{clk} = \begin{bmatrix} 1 & (t_k - t_{ref}) & (t_k - t_{ref})^2 \end{bmatrix}$

ESTIMATOR DESIGN

Once the linearized single measurement equation (8) is derived, the estimator can be established. The parameters to be estimated or 'states' include SV orbit parameters $\delta\mathbf{p}_i^{orb}$, SV clock $\tau_{i,k}$, RS clock model parameters $\mathbf{p}_i^{clk}$, and cycle ambiguities ${}^{i,j}\eta$. All of these states can be simultaneously estimated using either a *batch* and *Kalman filter* implementation. The states are estimated over T_{FIT} of 4 hours, using a 4 min sample period to avoid modelling correlation between samples due to RS multipath. In addition, to obtain observability, all the clock error states, including both SV and RS clocks, are measured with respect the clock of RS 1.

Batch Estimator

The batch estimator is established by stacking all code and carrier measurements over the fit interval T_{FIT}. Measurements for all SVs from 1 to *I* are collected by all RS from 1 to *J*, at all time epochs from 1 to *K*. The resulting estimation equation is written as:

$$\begin{bmatrix} {}^{1,1}\delta\boldsymbol{\rho}_K \\ {}^{1,2}\delta\boldsymbol{\rho}_K \\ \vdots \\ {}^{1,J}\delta\boldsymbol{\rho}_K \\ \vdots \\ {}^{i,j}\delta\boldsymbol{\rho}_K \\ \vdots \\ {}^{I,J}\delta\boldsymbol{\rho}_K \\ {}^{1,1}\delta\boldsymbol{\varphi}_K \\ \vdots \\ {}^{I,J}\delta\boldsymbol{\varphi}_K \end{bmatrix} = \left[\begin{array}{cccc:cccc:ccc:cccc} {}^{1,1}\mathbf{B}_K & \mathbf{0}_{K\times15} & \cdots & \mathbf{0}_{K\times15} & \mathbf{I}_{K\times K} & \mathbf{0}_{K\times K} & \cdots & \mathbf{0}_{K\times K} & \mathbf{0}_{K\times3} & \cdots & \mathbf{0}_{K\times3} & \mathbf{0}_{K\times1} & \cdots & \mathbf{0}_{K\times1} \\ {}^{1,2}\mathbf{B}_K & \mathbf{0}_{K\times15} & \cdots & \mathbf{0}_{K\times15} & \mathbf{I}_{K\times K} & \mathbf{0}_{K\times K} & \cdots & \mathbf{0}_{K\times K} & \mathbf{A}_{2,K}^{clk} & \cdots & \mathbf{0}_{K\times3} & \mathbf{0}_{K\times1} & \cdots & \mathbf{0}_{K\times1} \\ \vdots & \vdots & & \vdots & \vdots & \vdots & & \vdots & & \ddots & & \vdots & & \vdots \\ {}^{1,J}\mathbf{B}_K & \mathbf{0}_{K\times15} & \cdots & \mathbf{0}_{K\times15} & \mathbf{I}_{K\times K} & \mathbf{0}_{K\times K} & \cdots & \mathbf{0}_{K\times K} & \mathbf{0}_{K\times3} & \cdots & \mathbf{A}_{J,K}^{clk} & \mathbf{0}_{K\times1} & \cdots & \mathbf{0}_{K\times1} \\ & \ddots & & \vdots & & \ddots & & \vdots & \vdots & \ddots & & \vdots & & \vdots \\ \mathbf{0}_{K\times15} & {}^{i,j}\mathbf{B}_K & \cdots & \mathbf{0}_{K\times15} & \mathbf{0}_{K\times K} & \mathbf{I}_{K\times K} & \cdots & \mathbf{0}_{K\times K} & \mathbf{0}_{K\times3} & \mathbf{A}_{j,K}^{clk} & \cdots & \mathbf{0}_{K\times1} & \cdots & \mathbf{0}_{K\times1} \\ \vdots & & \ddots & & \vdots & & \ddots & & \vdots & & \ddots & \vdots & & \vdots \\ \mathbf{0}_{K\times15} & \cdots & \mathbf{0}_{K\times15} & {}^{I,J}\mathbf{B}_K & \mathbf{0}_{K\times K} & \cdots & \mathbf{0}_{K\times K} & \mathbf{I}_{K\times K} & \mathbf{0}_{K\times3} & \cdots & \mathbf{A}_{J,K}^{clk} & \mathbf{0}_{K\times1} & \cdots & \mathbf{0}_{K\times1} \\ {}^{1,1}\mathbf{B}_K & \mathbf{0}_{K\times15} & \cdots & \mathbf{0}_{K\times15} & \mathbf{I}_{K\times K} & \mathbf{0}_{K\times K} & \cdots & \mathbf{0}_{K\times K} & \mathbf{0}_{K\times3} & \cdots & \mathbf{0}_{K\times3} & \mathbf{1}_{K\times1} & \cdots & \mathbf{0}_{K\times1} \\ & & \ddots & & & & \ddots & & & & \ddots & & & \ddots \\ \mathbf{0}_{K\times15} & \cdots & \mathbf{0}_{K\times15} & {}^{I,J}\mathbf{B}_K & \mathbf{0}_{K\times K} & \cdots & \mathbf{0}_{K\times K} & \mathbf{I}_{K\times K} & \mathbf{0}_{K\times3} & \cdots & \mathbf{A}_{J,K}^{clk} & \mathbf{0}_{K\times1} & \cdots & \mathbf{1}_{K\times1} \end{array}\right] \begin{bmatrix} \delta\mathbf{p}_1^{orb} \\ \vdots \\ \delta\mathbf{p}_I^{orb} \\ \hdashline \boldsymbol{\tau}_{1,K} \\ \vdots \\ \boldsymbol{\tau}_{I,K} \\ \hdashline \mathbf{p}_2^{clk} \\ \vdots \\ \mathbf{p}_J^{clk} \\ \hdashline {}^{1,1}\eta \\ \vdots \\ {}^{I,J}\eta \end{bmatrix} + \begin{bmatrix} {}^{1,1}\boldsymbol{\varepsilon}_{\rho,K} \\ {}^{1,2}\boldsymbol{\varepsilon}_{\rho,K} \\ \vdots \\ {}^{1,J}\boldsymbol{\varepsilon}_{\rho,K} \\ \vdots \\ {}^{i,j}\boldsymbol{\varepsilon}_{\rho,K} \\ \vdots \\ {}^{I,J}\boldsymbol{\varepsilon}_{\rho,K} \\ {}^{1,1}\boldsymbol{\varepsilon}_{\varphi,K} \\ \vdots \\ {}^{I,J}\boldsymbol{\varepsilon}_{\varphi,K} \end{bmatrix} \quad (9)$$

Four groups of states are distinguished by the dashed thin lines. The notations are worth clarifying: $\mathbf{0}_{a\times b}$ is an $a\times b$ matrix of zeros, $\mathbf{1}_{a\times b}$ is an $a\times b$ matrix of ones, and $\mathbf{I}_{a\times a}$ is an $a\times a$ identity matrix. In addition, the product of LOS vector and Jacobian matrix in equation (8) is defined as ${}^{i,j}\mathbf{B}_k$, i.e., ${}^{i,j}\mathbf{B}_k = {}^{i,j}\mathbf{e}_k^T\,\mathbf{A}_{i,k}^{orb}$. Since measurements at all time epochs are incorporated in equation (9), we use capital '*K*' to denote the time sequence. Therefore,

$${}^{i,j}\delta\boldsymbol{\rho}_K = \begin{bmatrix} {}^{i,j}\delta\rho_1 \\ \vdots \\ {}^{i,j}\delta\rho_K \end{bmatrix},\ {}^{i,j}\mathbf{B}_K = \begin{bmatrix} {}^{i,j}\mathbf{B}_1 \\ \vdots \\ {}^{i,j}\mathbf{B}_K \end{bmatrix},\ \boldsymbol{\tau}_{i,K} = \begin{bmatrix} \tau_{i,1} \\ \vdots \\ \tau_{i,K} \end{bmatrix} \text{ and } {}^{i,j}\boldsymbol{\varepsilon}_{\rho,K} = \begin{bmatrix} {}^{i,j}\varepsilon_{\rho,1} \\ \vdots \\ {}^{i,j}\varepsilon_{\rho,K} \end{bmatrix} \quad (10)$$

It is obvious from equation (9) that this estimator is humongous due to the substantial number of measurements in the fit interval.

It is important to note that not all SVs will be visible to all RS during the fitting interval. To lighten the notations, these cases are not explicitly expressed in equations (9) and (10). But the corresponding rows must be removed whenever the measurements are unavailable.

Let us simplify equation (9) by defining $\mathbf{z}$, $\mathbf{H}$, $\mathbf{s}$, and $\boldsymbol{\varepsilon}$ to respectively be the measurement vector, observation matrix, state vector, and error vector. Then equation (9) becomes $\mathbf{z} = \mathbf{H}\mathbf{s} + \boldsymbol{\varepsilon}$, and the states can be evaluated using a weighted least-squares estimator:

$$\hat{\mathbf{s}} = \left(\mathbf{H}^T\mathbf{V}^{-1}\mathbf{H}\right)^{-1}\mathbf{H}^T\mathbf{V}^{-1}\mathbf{z} \tag{11}$$

where $\mathbf{V}$ is the covariance matrix of the measurement error vector $\boldsymbol{\varepsilon}$. The SV orbit parameters $\delta\mathbf{p}_i^{orb}$ and clock $\tau_{i,k}$ can be extracted from the full-state estimate vector $\hat{\mathbf{s}}$. Furthermore, the SV position is obtained by substituting the estimated orbit model parameters into equation (2).

Kalman Filter Approach

In addition to the batch estimator, we also provide a KF approach. The KF implementation is more computationally efficient, and it allows us to cross-check with the results from batch estimator. At one time epoch *k*, the measurement equation is expressed as:

$$\begin{bmatrix} {}^{1,1}\delta\rho_k \\ {}^{1,2}\delta\rho_k \\ \vdots \\ {}^{1,J}\delta\rho_k \\ \vdots \\ {}^{i,j}\delta\rho_k \\ \vdots \\ {}^{I,J}\delta\rho_k \\ {}^{1,1}\delta\varphi_k \\ \vdots \\ {}^{I,J}\delta\varphi_k \end{bmatrix} = \left[\begin{array}{ccc|ccc|ccc|cccc} {}^{1,1}\mathbf{B}_k & \cdots & \mathbf{0}_{1\times15} & 1 & \cdots & \mathbf{0}_{1\times K} & \mathbf{0}_{1\times3} & \cdots & \mathbf{0}_{1\times3} & 0\cdots0 & c_T & 0\cdots0 \\ {}^{1,2}\mathbf{B}_k & \cdots & \mathbf{0}_{1\times15} & 1 & \cdots & \mathbf{0}_{1\times K} & \mathbf{A}_{2,k}^{clk} & \cdots & \mathbf{0}_{1\times3} & 0\cdots0 & 0 & c_T & 0\cdots0 \\ \vdots & & \vdots & \vdots & & \vdots & & \ddots & & \vdots\ \vdots & \vdots & & \ddots \\ {}^{1,J}\mathbf{B}_k & \cdots & \mathbf{0}_{1\times15} & 1 & \cdots & \mathbf{0}_{1\times K} & \mathbf{0}_{1\times3} & \cdots & \mathbf{A}_{J,k}^{clk} & 0\cdots0 & 0\cdots0 & c_T \\ & \ddots & \vdots & & \ddots & & & \ddots & & \vdots\ \vdots & & \ddots & \\ \mathbf{0}_{1\times15} & {}^{i,j}\mathbf{B}_k\cdots & \mathbf{0}_{1\times15} & \mathbf{0}_{1\times K} & 1\cdots & \mathbf{0}_{1\times K} & \mathbf{0}_{1\times3} & \mathbf{A}_{j,k}^{clk}\cdots & \mathbf{0}_{1\times3} & 0\cdots0 & 0\ c_T & 0\cdots0 \\ \vdots & \ddots & & \vdots & \ddots & & & \ddots & & \vdots\ \vdots & \vdots & & \ddots \\ \mathbf{0}_{1\times15} & \cdots & {}^{I,J}\mathbf{B}_k & \mathbf{0}_{1\times K} & \cdots & 1 & \mathbf{0}_{1\times3} & \cdots & \mathbf{A}_{J,k}^{clk} & 0\cdots0 & 0\cdots0 & c_T \\ {}^{1,1}\mathbf{B}_k & \cdots & \mathbf{0}_{1\times15} & 1 & \cdots & \mathbf{0}_{1\times K} & \mathbf{0}_{1\times3} & \cdots & \mathbf{0}_{1\times3} & 1\cdots0 & c_T & 0\cdots0 \\ & \ddots & & & & & \vdots & \ddots & & & & \ddots & \\ \mathbf{0}_{1\times15} & \cdots & {}^{I,J}\mathbf{B}_k & \mathbf{0}_{1\times K} & \cdots & 1 & \mathbf{0}_{1\times3} & \cdots & \mathbf{A}_{J,k}^{clk} & 0\cdots1 & 0\cdots0 & c_T \end{array}\right] \left[\begin{array}{c} \delta\mathbf{p}_1^{orb} \\ \vdots \\ \delta\mathbf{p}_I^{orb} \\ \hline \boldsymbol{\tau}_{1,K} \\ \vdots \\ \boldsymbol{\tau}_{I,K} \\ \hline \mathbf{p}_2^{clk} \\ \vdots \\ \mathbf{p}_J^{clk} \\ \hline {}^{i,j}\eta \\ \hline \varepsilon_{tropo,1,k}^{ZTD} \\ \vdots \\ \varepsilon_{tropo,J,k}^{ZTD} \end{array}\right] + \begin{bmatrix} {}^{1,1}\varepsilon_{\rho,k}^{RNM} \\ {}^{1,2}\varepsilon_{\rho,k}^{RNM} \\ \vdots \\ {}^{1,J}\varepsilon_{\rho,k}^{RNM} \\ \vdots \\ {}^{i,j}\varepsilon_{\rho,k}^{RNM} \\ \vdots \\ {}^{I,J}\varepsilon_{\rho,k}^{RNM} \\ {}^{1,1}\varepsilon_{\varphi,k}^{RNM} \\ \vdots \\ {}^{I,J}\varepsilon_{\varphi,k}^{RNM} \end{bmatrix} \tag{12}$$

Compared with equation (9), the additional states $\varepsilon_{tropo,j,k}^{ZTD}$ in equation (12) represent the residual ZTD at RS *j*, and c_T is the obliquity factor. We use state augmentation to account for time correlation of the tropospheric ZTD error [16]. Because $\varepsilon_{tropo,j}^{ZTD}$ is modeled as a first order Gauss-Markov process (FOGMP), the associated dynamic model of the KF approach is expressed as:

$$\begin{bmatrix} \mathbf{s}_{k+1} \\ \boldsymbol{\varepsilon}_{tropo,k+1}^{ZTD} \end{bmatrix} = \begin{bmatrix} \mathbf{I} & \mathbf{0} \\ \mathbf{0} & e^{-T/\mu}\mathbf{I}_{J\times J} \end{bmatrix} \begin{bmatrix} \mathbf{s}_k \\ \boldsymbol{\varepsilon}_{tropo,k}^{ZTD} \end{bmatrix} + \begin{bmatrix} \mathbf{0} \\ \mathbf{1}_{J\times1} \end{bmatrix} \omega_{tropo,k}^{ZTD} \tag{13}$$

In equation (13), the first row accounts for the states in equation (9), which do not change over time. The second row shows the dynamics of FOGMP, where T is the sample period and μ is the time constant [17]. $\boldsymbol{\varepsilon}_{tropo,k}^{ZTD}$ is obtained by stacking $\varepsilon_{tropo,j,k}^{ZTD}$ of all RS, and the variance of $\omega_{tropo,k}^{ZTD}$ is $(1 - e^{-2(T/\mu)})\sigma_{ZTD}^2$ [18]. As a result, with both the measurement equation and dynamic model available, the nominal KF steps [16] can be implemented to estimate SV orbit/clock.

Up until now, the offline monitor's orbit and clock estimator has been fully established using two approaches, and the estimation process has been described in detail. The derivations of both approaches were done for the case where the legacy orbit model is

applied and RS clock errors are modeled using a quadratic polynomial. For cases when the CNAV orbit model is used or RS clocks are not modeled, the expressions of equations (9) and (12) need to be modified to accommodate the corresponding scenario.

There will be two error sources contributing the monitor's SV orbit/clock estimation error: (a) measurement error and (b) residual model error. To respectively address their impacts on the monitor's performance, we carry out two separate analyses: covariance analysis and model fidelity analysis.

COVARIANCE ANALYSIS

In this section, covariance analysis used to investigate the contribution of measurement error on $\sigma_{MONITOR}$. For illustrative purposes, we will employ the batch estimator equations to derive the covariance matrix of SV orbit/clock states. According to equations (9) and (11), the covariance matrix of the full-states $\boldsymbol{s}$ can be computed by:

$$\boldsymbol{\Sigma} = \left(\mathbf{H}^T \mathbf{V}^{-1} \mathbf{H}\right)^{-1} \tag{14}$$

To evaluate the position and clock estimate error covariance of SV i at time epoch k, we first build the covariance matrix of the SV orbit parameters and clock $\mathbf{D}_{i,k}$, by extracting corresponding elements from $\boldsymbol{\Sigma}$. Therefore, $\mathbf{D}_{i,k}$ is 16×16 if a legacy orbit model is employed. Then, the 4×4 covariance matrix $\mathbf{P}_{LL,i,k}$ of satellite position and clock in the local-level (LL) reference frame (along-track, cross-track, radial) can be evaluated by:

$$\mathbf{P}_{LL,i,k} = \begin{bmatrix} \mathbf{R}_{LL,i,k} & 0 \\ 0 & 1 \end{bmatrix} \mathbf{C}_{i,k} \mathbf{D}_{i,k} \mathbf{C}_{i,k}^T \begin{bmatrix} \mathbf{R}_{LL,i,k} & 0 \\ 0 & 1 \end{bmatrix}^T \tag{15}$$

where $\mathbf{R}_{LL,i,k}$ is the ECEF to LL rotation matrix, and $\mathbf{C}_{i,k}$ is defined as:

$$\mathbf{C}_{i,k} = \begin{bmatrix} \mathbf{A}_{i,k}^{orb} & 0 \\ 0 & 1 \end{bmatrix} \tag{16}$$

To investigate the SIS in range domain, we evaluate the maximum SISRE standard deviation at the worst-case user location. This is achieved by projecting $\mathbf{P}_{LL,i,k}$ along LOS for all locations within SV footprint [11]. And the worst-case SISRE standard deviation $\sigma^2_{SISRE,i,k}$ is defined as the maximum projection. In Figure 3, the projection region is shaded in light blue, and the black dashed line is one example projection line $\mathbf{G}_{i,m}$, where m is the index of the lines. Therefore, $\sigma^2_{SISRE,i,k}$ is evaluated by:

$$\sigma^2_{SISRE,i,k} = \max_{m=1,\ldots ALL} \left(\mathbf{G}_{i,m} \mathbf{P}_{LL,i,k} \mathbf{G}_{i,m}^T\right) \tag{17}$$

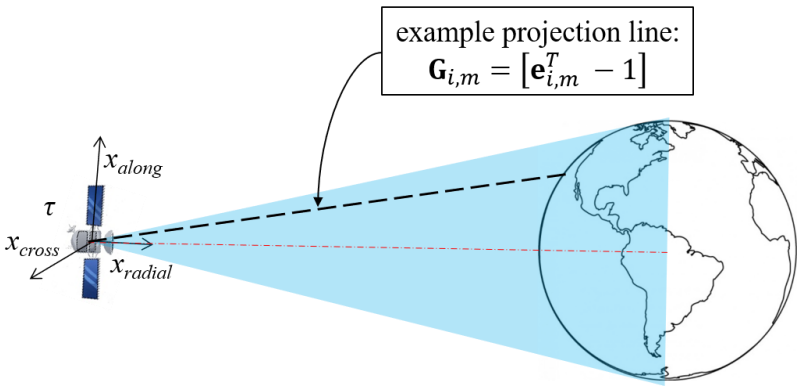

Fig. 3 Covariance Matrix Projections along LOS for All Locations

To explore the potential benefits of employing orbit/clock models to the estimation process, the covariance analyses are performed under 4 scenarios:

- CASE 1: legacy orbit model, quadratic RS clock model
- CASE 2: legacy orbit model, free RS clock states
- CASE 3: CNAV orbit model, quadratic RS clock model
- CASE 4: CNAV orbit model, free RS clock states

In the analyses, we take all measurements over the fitting interval T_{FIT} as one data set, with each data set starting at regular one-hour intervals over a day. SV positions are computed from a GPS almanac, which is typically applied in covariance analysis [7, 9].

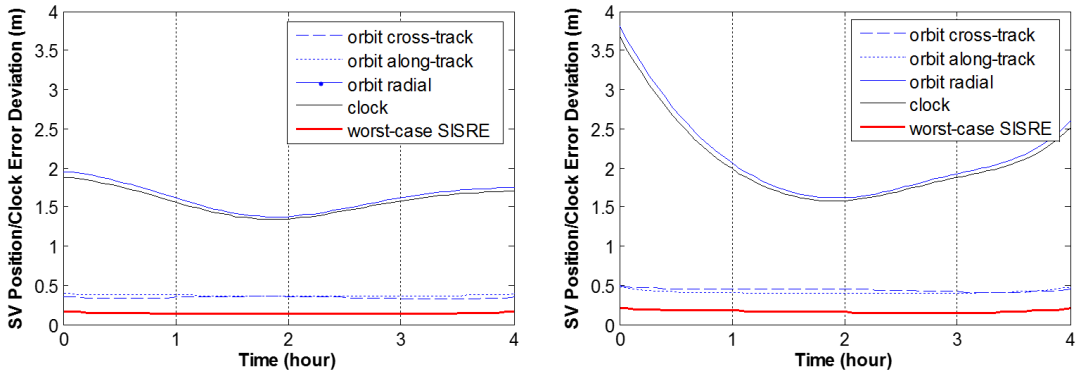

Fig. 4 Example Profiles of Error Deviations along One Fitting Interval for Case 1 (Left) and Case 4 (Right)

Figure 4 shows standard deviation profiles of an example satellite (PRN 5) over one fitting interval. Three light blue lines are the orbit error deviations of orbit along-track, cross-track, and radial. The black thin lines represent the satellite clock error deviation. The red thick lines are of greatest interest because they show the worst-case SISRE standard deviation, evaluated using equation (17). In both cases shown in the figure, the orbit radial and clock components are highly correlated, which results in significantly smaller σ_{SISRE} than each individual term. Comparing the two figures, even though the orbit radial and clock terms are increased for case 4, there is no noticeable difference between the two red lines. We take the central two-hour values as the final results of each fitting interval. Therefore, only the data between Hour 1 and Hour 3 in Figure 4 will be considered.

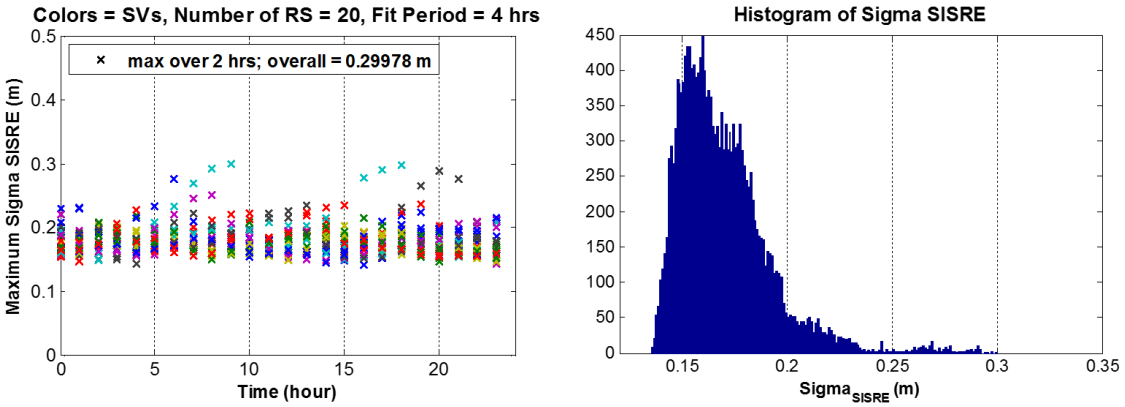

Fig. 5 Maximum σ_{SISRE} over One Day (Left) and Their Distribution (Right) for Case 4

The left plot of Figure 5 shows the maximum σ_{SISRE} profiles over a one-day period. Each column represents the largest σ_{SISRE} values of that fitting interval, and satellites are distinguished by different colors. The distribution of σ_{SISRE} is captured by the histogram on the right, which shows that a large majority σ_{SISRE} values are well below 0.25 m, and the maximum σ_{SISRE} is 0.3 m.

Table 1. Maximum σ_{SISRE} Values under Four Scenarios

	Quadratic Model for RS Clock	*Free RS Clock*
Legacy Orbit Model	CASE 1: 0.277m	CASE 2: 0.287m
CNAV Orbit Model	CASE 3: 0.283m	CASE 4: 0.30m

Table 1 summarizes the covariance analysis results by presenting the maximum σ_{SISRE} values of the four cases. At the first sight of this table, it can be observed that there are only small variations among those values. So, from the perspective of mitigating the contribution of measurement error on $\sigma_{MONITOR}$, no significant benefit can be obtained by using different orbit/clock models. As expected, case 4 results in the largest σ_{SISRE} because it has the largest number of unknown parameters to be estimated. Based on these results, we recommend not using a quadratic model for RS clock error since there is little benefit from it, and not using it simplifies the estimator and allows for seamless performance in the event of an RS clock fault (because clock errors are estimated at each epoch individually). Therefore, cases 1 and 3 are no longer investigated, and so it only remains to address the impact of orbit model error on the monitor's performance.

ORBIT MODEL FIDELITY ANALYSIS

In this section, the residual model error is evaluated for two candidate orbit models: legacy and CNAV. To do this, precise GPS orbit data is first fed as measurements into equation (2), and then the orbit parameters $\mathbf{p}_i^{orb}$ are estimated using a non-linear least squares algorithm [19]. IGS data $\mathbf{x}^{IGS}$ was employed as the truth orbit, and the CSP broadcast ephemeris $\bar{\mathbf{p}}_i^{orb}$ parameter vector was used as the initial guess in the estimation process. Once $\mathbf{p}_i^{orb}$ is estimated the residual error can be computed by subtracting $\mathbf{x}^{IGS}$ with the model's output. Therefore, for SV *i* at time epoch *k*, the ECEF residual is:

$$\mathbf{r}_{i,k} = \mathbf{x}_{i,k}^{IGS} - \mathbf{g}_{orb,k}(\hat{\mathbf{p}}_i^{orb}) \tag{18}$$

where $\hat{\mathbf{p}}_i^{orb}$ is the estimated orbit parameter vector. Finally, $\mathbf{r}_{i,k}$ can be expressed in the LL frame as:

$$\mathbf{r}_{LL,i,k} = \mathbf{R}_{LL,i,k}\mathbf{r}_{i,k} = [r_{A,i,k} \quad r_{C,i,k} \quad r_{R,i,k}]^T \tag{19}$$

In equation (19), the three components of the last vector represent the residual error in three dimensions: along-track, cross-track, and radial. To evaluate the ranging error from $\mathbf{r}_{LL,i,k}$, multiple analytical expressions can be found in the literature [12], [20-22]. In this paper, we consider the following equation for orbit-only SISRE:

$$r_{SISRE,i,k} = 0.98 r_{R,i,k} + 0.24\,\mathrm{sgn}(r_{R,i,k})\sqrt{r_{A,i,k}^2 + r_{C,i,k}^2} \tag{20}$$

Equation (20) is very similar to the one in [20], except the SV clock term is removed. The derivation can be found in the reference and will not be restated here.

This analysis utilizes IGS data of the first ten days of 2016, i.e., 01/01/2016 - 01/10/2016. Similar to the covariance analysis, the data is fit to the model over T_{FIT} of 4 hours, and each fitting interval starts at 2 hours over a day. The sample period is 15 mins, and only the 2-hour central results are recorded.

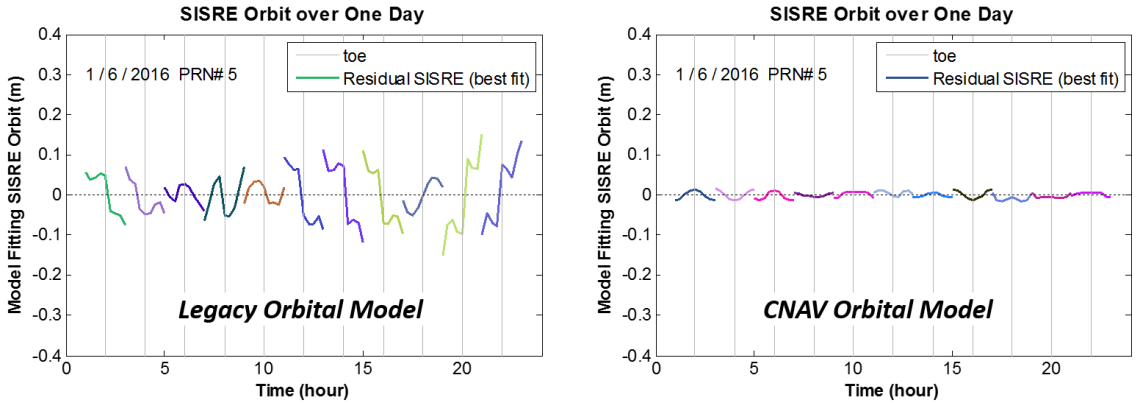

Fig. 6 Best Fit Residual SISRE Orbit over One Day

Figure 6 shows the residual SISRE error for an example SV (PRN 5) on 01/06/2016. In each individual figure, the color-code helps distinguish fit intervals. Vertical t_{oe}-lines indicate the time of ephemeris, which is at the center of each 2-hour window. The results show that the residual SISRE of CNAV orbit model is significantly smaller than that of legacy orbit model.

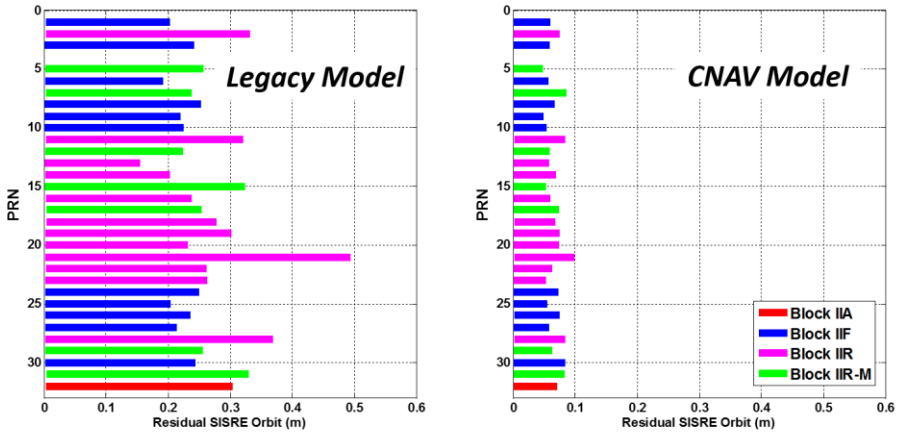

Fig. 7 Residual SISRE Orbit Ranges

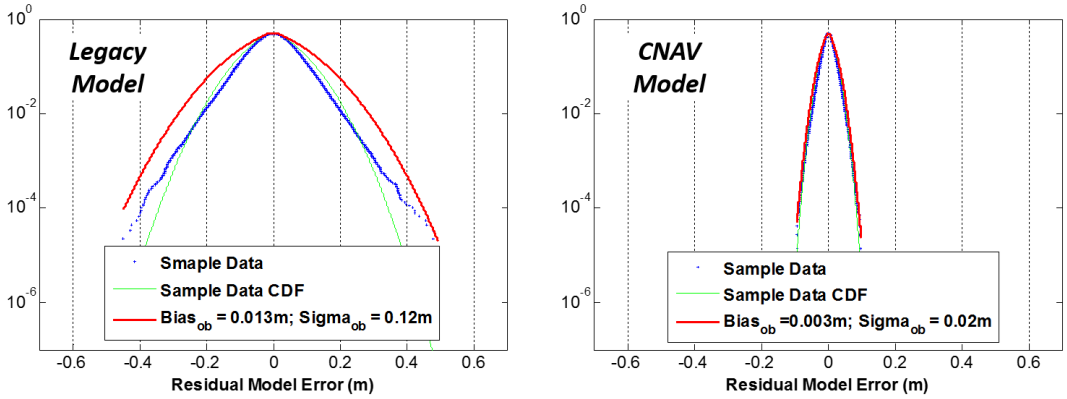

Fig. 8 Residual SISRE Orbit Overbound

Figures 7 and 8 provide a more general view of the residual SISRE profile by processing all of the IGS data. The SISRE ranges in Figure 7 are expressed in terms of GPS SV blocks. Using the GPS legacy orbit model, the maximum SISRE is 0.5 m and SISRE

root-mean-square (RMS) is 0.089 m. These two values are respectively reduced to 0.1 m and 0.022 m with the CNAV model. In Figure 8, the data is overbounded using a Gaussian distribution with mean at b_{ob} and standard deviation of σ_{ob}. By comparing the two orbit models, it can be observed that employing the CNAV model will dramatically reduce the residual error. The CNAV model fidelity error can be quantified using a Gaussian bound with approximately zero-mean, 2 cm standard deviation, which does not cause a significant contribution to the monitor's orbit/clock error. Given that contribution of CNAV model error is negligible compared to the effect of measurement error shown in Table 1, and that the same is not true for the legacy model, it is recommended to use the CNAV orbit model for the ARAIM offline monitor's orbit estimator.

CONCLUSION

This paper describes the design, analysis, and evaluation of an ARAIM offline ground monitor, which aims at validating the ISM broadcast to the users. The monitor employs a network of worldwide sparsely distributed reference stations (RS) and a parametric orbit model to simultaneously estimate SV orbits, SV clocks, and RS clocks. Two estimators are derived, and their implementation is described in detail in the paper. Covariances and model fidelities are analyzed to assess the impact of RS measurement error and model fitting error on the monitor's performance: the most robust implementation with the overall lowest SV orbit/clock errors is achieved by making no assumptions on SV or RS clock dynamics and by using the CNAV orbit model. This monitor is predicted to achieve a signal in space range error standard deviation $\sigma_{MONITOR}$ of about 0.3 m, which will allow validation ARAIM user range accuracies σ_{URA} of 1.05 m if the actual σ_{URA} is 1 m. In the next steps of this work, we will use experimental data to validate the design of the offline monitor.

ACKNOWLEDGEMENT

The authors would like to thank the Federal Aviation Administration for sponsoring this work. However, the views and opinions expressed in this paper are those of the authors and do not necessarily reflect those of any other organization or person.

REFERENCES

[1] Pervan, B., "Navigation integrity for aircraft precision landing using the global positioning system," Ph.D. Dissertation, Dept. of Aeronautics and Astronautics, Stanford Univ., Stanford, CA, 1996.

[2] Lee, Y. C., "Analysis of Range and Position Comparison Methods as a Means to Provide GPS Integrity in the User Receiver," *Proceedings of the 42nd Annual Meeting of The Institute of Navigation,* Seattle, WA, 1986, pp. 1-4.

[3] Parkinson, B. W., and Axelrad, P., "Autonomous GPS Integrity Monitoring Using the Pseudorange Residual," *NAVIGATION: Journal of the Institute of Navigation,* Vol. 35, No. 2, 1988, pp. 255–274.
doi:10.1002/j.2161-4296.1988.tb00955.x

[4] RTCA Special Committee 159, "Minimum Operational Performance Standards for Airborne Supplemental Navigation Equipment Using Global Positioning System (GPS)," RTCA/DO-208, July 1991.

[5] Joerger, M., Chan, F.-C., and Pervan, B., "Solution Separation Versus Residual-Based RAIM," *NAVIGATION: Journal of the Institute of Navigation,* Vol. 61, No. 4, Winter 2014, pp. 273-291.
doi: 10.1002/navi.71

[6] Gibbons, G., "Munich Summit Charts Progress of GPS, GLONASS, Galileo, Beidou GNSSes," Inside GNSS, March 20, 2012.

[7] Blanch, J., Walter, T., Enge, Per., Lee, Y., Pervan, B., Rippl, M., Spletter, A., and Kropp, V., "Baseline Advanced RAIM User Algorithm and Possible Improvements," *IEEE Transactions on Aerospace and Electronic Systems,* Vol 51, January 2015, pp. 713-732.
doi: 10.1109/TAES.2014.130739

[8] Phase II of the GNSS Evolutionary Architecture Study, February 2010. URL:

https://www.faa.gov/about/office_org/headquarters_offices/ato/service_units/techops/navservices/gnss/library/documents/media/GEASPhaseII_Final.pdf

[9] EU-U.S. Cooperation on Satellite Navigation, Working Group C, "ARAIM Technical Subgroup Milestone 2 Report," February 11, 2015. URL:
http://www.gps.gov/policy/cooperation/europe/2015/working-group-c/

[10] Blanch, J., et al, "Architectures for Advanced RAIM: Offline and Online," *Proceedings of the 27th International Technical Meeting of The Satellite Division of the Institute of Navigation (ION GNSS+ 2014)*, Tampa, Florida, September 2014, pp. 787-804.

[11] Walter, T., Blanch, J., "Keynote: Characterization of GNSS Clock and Ephemeris Errors to Support ARAIM," *Proceedings of the ION 2015 Pacific PNT Meeting*, Honolulu, Hawaii, April 2015, pp. 920-931.

[12] Perea, S., Meurer, M., Rippl, M., Belabbas, B., and Joerger, M., "URA/SISA Analysis for GPS and Galileo to Support ARAIM," *NAVIGATION: Journal of the Institute of Navigation*, Vol. 64, No. 2, Summer 2017, pp. 237-254.
doi: 10.1002/navi.199.

[13] Walter, T., Gunning, K., Blanch, J., "Keynote: Validation of the Unfaulted Error Bounds for ARAIM," *Proceedings of the ION 2017 Pacific PNT Meeting*, Honolulu, Hawaii, May 2017, pp. 1-19.

[14] Joerger, M., Zhai, Y., Pervan, B., "Online Monitor Against Clock and Orbit Ephemeris Faults in ARAIM," *Proceedings of the ION 2015 Pacific PNT Meeting*, Honolulu, Hawaii, April 2015, pp. 932-945.

[15] Global Positioning System Directorate Systems Engineering and Integration, "Interface Specification IS-GPS-200," Revision H, 2013. URL:
http://www.gps.gov/technical/icwg/IS-GPS-200H.pdf

[16] Brown, R. G., Hwang, P. Y. C., "*Introduction to Random Signals and Applied Kalman Filtering,*" 4th Ed, Wiley, 2012.
ISBN: 978-0-470-60969-9

[17] Gelb, A., "*Applied Optimal Estimation*," the MIT Press, 2001.
ISBN: 0-262-57048-3

[18] Joerger, M., "Carrier Phase GPS Augmentation Using Laser Scanners and Using Low Earth Orbiting Satellites," Ph.D. Dissertation, Dept. of Mechanical, Materials, and Aerospace Engineering, Illinois Institute of Technology, Chicago, IL, 2009.

[19] Crassidis, J., Junkins, J., "Optimal Estimation of Dynamic Systems," Chapman & Hall/CRC, 2004.
ISBN: 1-58488-391-X

[20] Heng, L., "Safe Satellite Navigation with Multiple Constellations: Global Monitoring of GPS and GLONASS Signal-In-Space Anomalies," Ph.D. Dissertation, Dept. of Aeronautics and Astronautics, Stanford Univ., Stanford, CA, 2012.

[21] Malys, S., et al, "The GPS Accuracy Improvement Initiative," *Proceedings of the 10th International Technical Meeting of the Satellite Division of The Institute of Navigation (ION GPS 1997)*, Kansas City, MO, September 1997, pp. 375-384.

[22] Assistant Secretary of Defense for Command, Control, Communications and Intelligence. "Global Positioning System Standard Positioning Service Performance Standard." Washington, DC, 2008. URL:
http://www.gps.gov/technical/ps/2008-SPS-performance-standard.pdf